energies

MDPI

Article

Response of Non-Polar Oil Component on Low Salinity Effect in Carbonate Reservoirs: Adhesion Force Measurement Using Atomic Force Microscopy

Nasser S. Al Maskari [1,2,*], Ahmad Sari [1], Md Mofazzal Hossain [1], Ali Saeedi [1] and Quan Xie [1,*]

[1] Discipline of Petroleum Engineering, WA School of Mines: Minerals, Energy and Chemical Engineering, Curtin University, 26 Dick Perry Avenue, Kensington, WA 6151, Australia; ahmad.sari@postgrad.curtin.edu.au (A.S.); md.hossain@curtin.edu.au (M.M.H.); Ali.Saeedi@curtin.edu.au (A.S.)

[2] Petroleum Development Oman LLC, P.O. Box 81, Code 100, Muscat, Sultanate of Oman

* Correspondence: n.almaskari1@postgrad.curtin.edu.au (N.S.A.M.); quan.xie@curtin.edu.au (Q.X.)

Received: 27 November 2019; Accepted: 17 December 2019; Published: 22 December 2019

Abstract: While the effect of polar-oil component on oil-brine-carbonate system wettability has been extensively investigated, there has been little quantitative analysis of the effect of non-polar components on system wettability, in particular as a function of pH. In this context, we measured the contact angle of non-polar oil on calcite surface in the presence of 10,000 ppm NaCl at pH values of 6.5, 9.5 and 11. We also measured the adhesion of non-polar oil group ($-CH_3$) and calcite using atomic force microscopy (AFM) under the same conditions of contact angle measurements. Furthermore, to gain a deeper understanding, we performed zeta potential measurements of the non-polar oil-brine and brine-calcite interfaces, and calculated the total disjoining pressure. Our results show that the contact angle decreases from 125° to 78° with an increase in pH from 6.5 to 11. AFM measurements show that the adhesion force decreases with increasing pH. Zeta potential results indicate that an increase in pH would change the zeta potential of the non-polar oil-brine and calcite-brine interfaces towards more negative values, resulting in an increase of electrical double layer forces. The total disjoining pressure and results of AFM adhesion tests predict the same trend, showing that adhesion forces decrease with increasing pH. Our results show that the pH increase during low-salinity waterflooding in carbonate reservoirs would lift off non-polar components, thereby lowering residual oil saturation. This physiochemical process can even occur in reservoirs with low concentration of polar components in crude oils.

Keywords: low salinity water; non-polar oil; carbonate; AFM; contact angle; zeta potential

1. Introduction

Carbonate reservoirs host roughly >60% of hydrocarbons (oil and gas) in the world [1], but only up to 40% of the oil can be recovered from the reservoirs [2]. The petroleum industry is therefore constantly working to develop economically feasible techniques to enhance oil recovery in order to meet the growing global demand for energy [3]. One technique that has attracted interest within the industry is low-salinity water flooding [4]. Extensive research has been done to show that lowering injected brine salinity can improve oil recovery from carbonate reservoir at secondary and tertiary mode from 5 to 30% of the original oil in place (OOIP) [5–12]. Wettability alteration towards a more water-wet state is believed to be one of the main physiochemical processes behind the low salinity effect, which shifts oil relative permeability towards a lower residual oil saturation [9,13–15], thus

enhancing oil recovery. To understand the factors controlling the wettability alteration process in carbonate reservoirs, several explanations have been developed and proposed to predict and quantify the wettability alteration, such as electrostatic bridging [7,8,16–18], electrical double layer [13,19–21], and surface complexation modelling [22,23].

To be more specific, the existing literature shows that the adsorption of the sulphate onto the pore surface would likely shift the surface charge from positive to negative, thus leading to a repulsion force between the oil (base and acidic functional groups) and carbonate pore surfaces [7]. Additionally, previous studies show that electrical double layer force also plays an important role in wettability alteration and release of the oil component from the carbonate surface [13,18,20,21,23]. For example, Mahani et al. [18] measured the zeta potential of the oil-brine and brine-carbonate (limestone) interfaces. They found that decreasing the salinity leads to an increase in the negative charge of the polar oil-brine and brine-carbonate (limestone) interfaces, suggesting a weaker electrostatic adhesion between the polar oil-brine and brine-carbonate (limestone) interfaces, and hence recession of the three-phase contact line. Furthermore, to gain a deeper understanding at the molecular level, atomic force microscopy (AFM) [24,25] and quartz crystal microbalance (QCM) [26] have been used to examine the effect of brine chemistry on polar oil-rock adhesion. For example, Liu et al. [24] used AFM to study the effect of salinity on the adhesion force between functional oil groups and hydrophobic surfaces. They concluded that the electrical double layer was at least one of the controlling factors of adhesion forces, and thus the wettability of oil-brine-rock. In addition, Joonaki et al. [26] used QCM to investigate the impact of brine composition on the deposition of the asphaltene oil species on the rock surface at elevated temperature and pressure conditions. They found that brine composition and salinity play an important role in the deposition of the asphaltene oil species on the rock surface, thereby affecting the wettability of the oil-brine-rock system.

To better quantify and predict the wettability alteration process, surface complexation modelling has been implemented to model chemical surface species from oil and calcite surfaces, thus characterizing the adhesion of oil and calcite [22,23,27–30]. For example, Brady et al. [22] developed a surface complexation model to characterize the wettability of oil-brine-calcite using a bond product sum concept, which is equal to $[–NH^+]\,[>CO_3^-] + [–NH^+]\,[>CaCO_3^-] + [–COOCa^+]\,[>CO_3^-] + [–COOCa^+]\,[>CaCO_3^-] + [–COO^-]\,[>CaOH_2^+] + [–COO^-]\,[>CO_3Ca^+]$. They suggest that the potential adhesion between the polar oil and carbonate surface increases with increasing bond product (more oil-wet system), and the potential adhesion between the polar oil and carbonate surface decreases with decreasing bond product (less oil-wet system). However, the above geochemical models were proposed to characterize oil-brine-carbonate wettability in light of the interaction of polar oil groups ($–NH^+$ and $–COO^-$) on carbonate surfaces. Few research have been done to draw on any structured research into the response of non-polar oil on wettability alteration when low-salinity waterflooding in carbonate reservoirs, and fewer works have been performed to investigate the effect of pH on the adhesion of non-polar oil and calcite, although local pH likely increases with low-salinity water flooding in carbonate reservoirs [31–34]. For example, Generosi et al. [35] used AFM to investigate the effect of the potential determining ions on the calcite wettability, although the pH effect was not examined. They found that the presence of Mg^{2+} and SO_4^{2-} ions decreased the adhesion forces between CH_3-terminated tip and calcite surface, thus increasing hydrophilicity.

In conclusion, while the influence of polar oil components on wettability alteration has been extensively investigated, in particular in geochemical modelling and molecular-level force measurements, researchers have not treated the response of non-polar oil on wettability alteration in much detail. Also, we know that the binding/bridging between polar oil component-calcite surface would likely decrease with increasing pH, but how non-polar oil responds to the increase in pH remains unclear. We therefore hypothesized that non-polar oil would be lifted off from calcite surfaces due to the increase in pH during low-salinity water flooding. To test this hypothesis, we measured the contact angle of non-polar oil on the calcite surface in the presence of an aqueous ionic solution (10,000 ppm NaCl) at pH values of 6.5, 9.5, and 11. We also measured the adhesion of the non-polar oil

group ($–CH_3$) and calcite using AFM under the same conditions of the contact angle measurement. Furthermore, to gain a deeper understanding of the isothermal thermodynamic, we performed zeta potential measurements of $–CH_3$-brine and brine-calcite interfaces, and calculated the total disjoining pressure using a sphere to flat thermodynamic model under constant potential condition.

2. Experimental Procedures

2.1. Materials

2.1.1. Brine

To validate our hypothesis and study the influence of pH on the adhesion force between non-polar oil and carbonate surface, we used NaCl salt (Analytical reagent, 99.9%) and ultrapure water (Resistivity 18.2 MΩ) to prepare NaCl brine with 10,000 ppm salinity. It is noteworthy that divalent cations (Ca^{2+} & Mg^{2+}) were not used in this study because of their competition with H^+/OH^- to adsorb on calcite surfaces, which likely compensates for the pH effect on non-polar oil [36]. Rather, the monovalent ion can better help us to focus on the pH effect. Also, to avoid any variation of the pH due to calcite dissolution during the measurements, a piece of calcite crystal was submerged in the solution for two days to reach calcite dissolution equilibrium. It is worth noting that calcite dissolution can reach equilibrium within 4 h [37]. Finally, we used 0.250 mol/L of hydrochloric acid and sodium hydroxide solutions to adjust the pH of the brine to 9.5 and 11.

2.1.2. Oil

Given that this work aims to understand the response of non-polar component on the adhesion at calcite surface with the presence of various brines, we used model oil compound containing $–CH_3$ groups to represent hydrocarbon functional groups [27,38,39]. In this work, we used Octadecane ($C_{18}H_{38}$) for contact angle measurements, and 1-Octadecanethiol ($C_{18}H_{38}S$) for AFM measurements. The strong chemisorption of the thiol group on the gold helps to represent the oil on the gold AFM tip [40,41].

2.1.3. Calcite

To examine our hypothesis, we used calcite crystal (Iceland Spar from Ward's Science) as substrates for the contact angle measurements and the AFM experiments. To ensure the integrity of experimental measurements, and to avert the surface roughness effect on the contact angle and AFM measurements [42,43], the calcite crystals were cleaved to obtain a new clean smooth calcite surface [29], then rinsed with deionized water saturated with calcite to remove any small calcite pieces. It is worth noting that we saturated the deionized water with calcite to prevent any effect on the new calcite surface during cleaning. Also, it is noteworthy that the surface roughness of the new calcite surface used in this work is in a range of 4 to 7 nm, which has been reported in our previous work [44].

Also, we prepared calcite powders with diameters in the range of 10 to 100 μm for the zeta potential measurements at the interface of brine-calcite as a function of pH (6.5, 9.5 and 11). The calcite powders were prepared using the following steps. Deionized water saturated with calcite was used to clean the calcite crystal. Then, the calcite crystal was kept in an oven at 60° to remove any adsorbed water at surfaces. Afterwards, mortar and pestle were used to crush the calcite crystal to fine powders [21].

2.2. Contact Angle Measurements

In this study, we used the sessile drop method (Figure 1) to measure the contact angle of non-polar oil in the presence of aqueous ionic solution (10,000 ppm NaCl) at pH values of 6.5, 9.5 and 11 on calcite crystal surfaces. Given that pressure likely plays a negligible role in the oil-brine-rock system interactions [45], we measured the contact angle at ambient pressure. Also, we performed the contact angle measurements at 27 °C to avoid any solidification of the non-polar oil (Octadecane). However,

a clean and new calcite substrate was used in the contact angle experiments. The substrate was obtained by cleaving a clean calcite sample, which was then rinsed with ultrapure water pre-saturated with $CaCO_3$ to remove all the remaining small pieces of calcite from the new surface. Afterward, the new calcite surface was placed into the wettability measurement cell which was pre-filled with NaCl solution. After that, a droplet of the non-polar oil was then introduced onto the calcite substrate using a syringe. The contact angle was monitored and recorded until the contact angle variation with time was negligible. It is worth noting that to solely focus on the pH effect on non-polar oil adhesion on calcite surfaces, and to compare contact angle results with adhesion force measured by atomic force microscopy, we did not use a porous carbonate rock to measure contact angle [46].

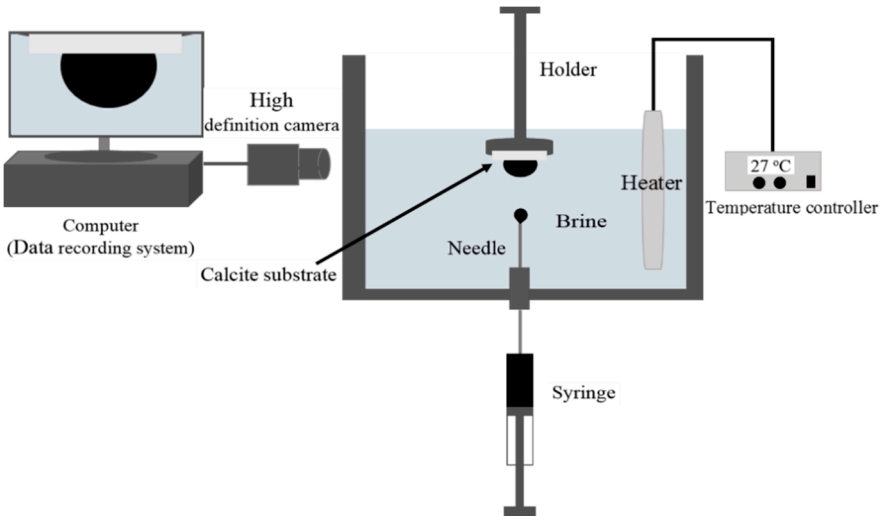

Figure 1. Schematic diagram of the contact angle test setup.

2.3. AFM Measurements

Atomic force microscopy (AFM) is an effective tool for directly measuring the adhesion force of the oil-brine-rock system [24,25,47–52]. In this work, we used AFM (WITec alpha 300 SAR) to measure the adhesion force between the model oil compound and calcite in the presence of NaCl brine (10,000 ppm) at pH values of 9.5 and 11 at ambient conditions. It is worth noting that we did not measure the adhesion force at pH 6.5 due to the fact that calcite dissolution at the surface may significantly affect the oil-brine-calcite adhesion at nano-scale. To achieve realistic adhesion force results, we performed about one thousand force-distance measurements for each of the experiments with one thousand data points for each force-distance curve. The mean average value is reported in the results section. However, WITec ProjectFOUR software was used to collect the AFM experimental data. Also, we modified the MatLab program developed by Yu et al. [53], and used it to extract adhesion force data for multiple measurements at the same time.

To functionalize the model oil compound onto the AFM tip surface, in all the AFM experiments, we used the AFM tips (NPG-10 from Bruker Corporation) coated with gold and with a spring constant of 0.06 N/m. A chemical (1-Octadecanethiol, $C_{18}H_{38}S$) was used to functionalize the tip to represent the non-polar oil group (–CH_3) [52]. To successfully functionalize the tip, we firstly used a plasma cleaner to clean the AFM tip for 30 min. Then, we immersed the AFM tip directly into ethanol at ambient temperature to minimize the gold oxide (Au_2O_3) that forms during the cleaning to metallic gold (Au) [54]. Thereafter, we submerged the AFM tip in 1mM of 1-Octadecanethiol ($C_{18}H_{38}S$) ethanol solution for one day. On the completion of the functionalization, the functionalized tip was washed by pure ethanol, and then dried by a stream of nitrogen gas prior to AFM measurements [55].

2.4. Zeta Potential Measurements

Electrical double layer force may play an important role in the wettability alteration of oil-brine-mineral systems [21,56,57], and this can be computed using the zeta potential of the oil-brine and brine-mineral interfaces. Thus, we used a Malvern Zetasizer ZS Nano series to measure the zeta potential of $-CH_3$-brine and brine-calcite interfaces at different pH values (6.5, 9.5 and 11). However, the zeta potential experiment methodologies are well demonstrated by Yang et al. [58]. It is worth noting that all the measurements were conducted at 27 °C, and the value of each zeta potential was taken from the mean average of four measurements.

2.5. Total Disjoining Pressure

To expand our understanding of the isothermal thermodynamic, we calculated the intermolecular forces (IMF) between the non-polar oil-brine and brine-calcite interfaces using Derjaguin, Landau, Verwey, and Overbeek (DLVO) theory [59,60].

$$\prod_{(\text{Total})} = \prod_{(\text{Van der Waals})} + \prod_{(\text{electric double layer})} + \prod_{(\text{structural})} \tag{1}$$

To interpret the AFM adhesion measurements better, we used the sphere to flat geometry model to compute the total disjoining pressure at the constant potential condition [52]. It is worth noting that our previous study showed that the sphere to flat geometry model could better interpret the adhesion between the tip and flat substrate in AFM experiments compared to flat to flat geometry model [52].

2.5.1. Van der Waals Forces

Van der Waals force is a long-range interaction, and it can be an attractive or repulsive force, depending on the sign of the calculated Hamaker constant [61]. In this research, the Van der Waals intermolecular force was an attractive force, and we computed the Van der Waals intermolecular force using the sphere to flat surface geometry model using the following model [61]:

$$\prod_{(\text{Van der Waals})} = -\frac{AR}{6h^2} \tag{2}$$

where R is the sphere radius (m), h the film thickness between the tip and flat substrate (m), and A is the Hamaker constant (range between 10^{-21} to10^{-19}) calculated using Equation (3), below [36]:

$$A = \frac{3}{4}k_B T\left(\frac{\varepsilon_o - \varepsilon_w}{\varepsilon_o + \varepsilon_w}\right) \times \left(\frac{\varepsilon_s - \varepsilon_w}{\varepsilon_s + \varepsilon_w}\right) \tag{3}$$

where k_B is the Boltzman constant (1.381×10^{-23} J·K^{-1}); T is the temperature in kelvin; ε_o is the permittivity of oil (2·C·V^{-1}·m^{-1}) [36]; ε_w is the permittivity of water (78.3 C·V^{-1}·m^{-1}), and ε_s is the permittivity of rock (7 C·V^{-1}·m^{-1}) [36].

2.5.2. Electric Double Layer Forces

Electric double layer forces are a function of the surface charges and brine ionic strength, which strongly affects the total disjoining pressure [59]. It is noteworthy that we calculated electrostatic potential using the Debye-Huckel equation although some of our zeta potential values are a bit greater than 50 mV [62].

$$\prod_{(\text{Electric double layer})} = \frac{2\pi R\varepsilon\varepsilon_w k\left[2\psi_1\psi_2 - \left(\psi_1^2 + \psi_2^2\right)e^{-kh}\right]}{\left(e^{+kh} - e^{-kh}\right)} \tag{4}$$

where ψ_1 and ψ_2 are the zeta potential of the brine-calcite and $-CH_3$-brine interfaces, respectively; ε is the permittivity of vacuum (8.85×10^{-12} C·V^{-1}.m^{-1}); R is the radius of the sphere (m), and k is the Debye length of solution (m^{-1}).

The Debye length is computed using equation 5 below [59]:

$$k^{-1} = \sqrt{\frac{\varepsilon \varepsilon_w \, k_B T}{2e^2 z^2 n_b}} \tag{5}$$

where e is the electron charge (1.60×10^{-19} C); z is the valence of a symmetrical electrolyte solution; and n_b is the ion density in the bulk solution.

2.5.3. Structural Forces

The structural forces are a short-range interaction ($h < 5$ nm) compared to the long-range interaction forces (Van der Waals and Electric double layer forces). In this research, the structural forces were attractive interaction (hydrophobic forces) [60,63], and we computed these using Equation (6), below [63]:

$$\prod_{(\text{structural})} = -A_s \exp\left(-\frac{h}{\lambda_0}\right) \tag{6}$$

where A_s is the constant range between 10^6 to 5×10^8 Pa [64]; and λ_0 is the structural forces decay length range between 0.2 to 1 nm [64]. In our study, we assumed that $A_s = 10^8$ Pa [64] and the λ_0 = 0.3 nm [65,66].

3. Results and Discussion

3.1. Effect of pH on the Contact Angle of the Non-Polar Oil-Brine-Calcite System

Our contact angle measurement (measured from the brine phase) shows that increasing the pH of the bulk brine leads to a decrease in the contact angle of the non-polar oil-brine-calcite system, indicating a more water-wet system. For example, Figure 2 shows that the contact angle of the non-polar oil-brine-calcite system decreases from 125° to 97° when pH increases from 6.5 to 9.5, and decreases further to 78° when the pH increases to 11. This is largely due to the fact that pH influences the magnitude and polarity of electrostatic forces at the non-polar oil-brine and brine-calcite interfaces [28,29]. Our results are in agreement with Rezaei et al. [67], who reported that increasing the pH of n-decane (non-polar oil)-brine-calcite system from 5 to 10 reduces the contact angle from 148° to 51°, suggesting that the wettability of n-decane-brine-calcite system is dependent on pH. Alameri et al. [13] also reported a similar pH effect on the contact angle of the oil-brine-carbonate system. It is also worth noting that pH likely significantly affects the interaction of the polar-oil-brine-carbonate system, and thus contact angle and wettability. For example, Xie et al. [29] found that increasing the pH from 3 to 8 increased the contact angle of the oil-brine (Na_2SO_4)-carbonate system from 53° to 175°. Moreover, the trend of the contact angle variation with pH can be predicted by the concept of bond product sum [28,29].

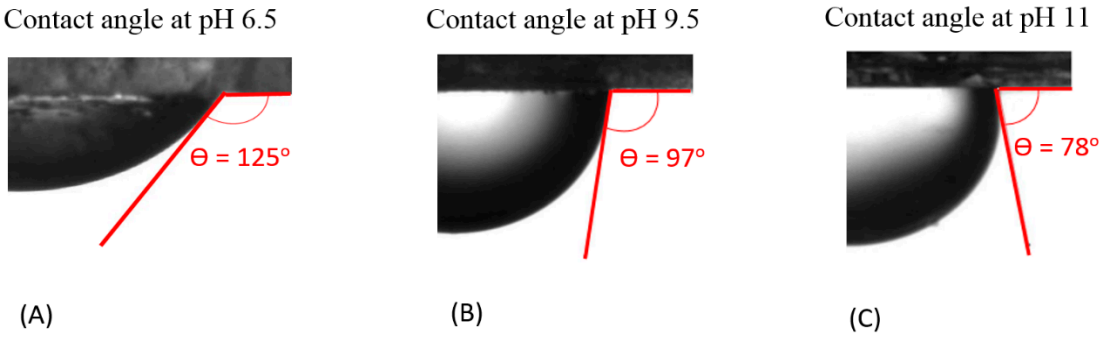

Figure 2. Contact of non-polar oil group ($-CH_3$) with calcite in the presence of NaCl solution at (**A**) pH 6.5, (**B**) pH 9.5, and (**C**) pH 11.

3.2. *Effect of pH on Non-Polar Oil-Calcite Interaction*

The AFM results show that the adhesion force between non-polar-oil and calcite decrease with increasing pH (Figures 3 and 4), supporting our contact angle measurements and confirming that the increase of pH caused by low-salinity injection likely prompts non-polar oil lifting off from pore surfaces. Figure 3 shows the average force-distance curves between non-polar oil group and calcite in the presence of sodium chloride brine (10,000 ppm salinity) at pH 9.5 and 11. The force-distance curves show that the adhesion forces of the non-polar oil group ($–CH_3$) decreases from about 9.2 to 2.8 nN (a 3-fold decrease) with an increase in pH from 9.5 to 11. While few studies have been done to examine the impact of pH on non-polar calcite adhesion with the aid of AFM, our new results are in agreement with our previous work [52], where we found that increasing the pH from 7 to 11 would decrease the adhesion force five times (from 890 to 180 pN) between non-polar oil ($–CH_3$) and muscovite in the presence of sodium chloride brine with 10,000 ppm salinity. Also, Juhl et al. [62] found that increasing the pH from 2 to 8 decreased the adhesion force between non-polar oil ($–CH_3$) and muscovite from 1200 to 100 pN. Additionally, they noticed a similar pH impact on the adhesion force between non-polar oil ($–CH_3$) and quartz. For example, in their measurements, when increasing the pH from 2 to 8, the adhesion force between the non-polar oil ($–CH_3$) and quartz decreased from 300 to ≈10 pN. Therefore, we tentatively conclude that increasing the pH increases the negative charges of the non-polar oil ($–CH_3$)-brine interface and brine-calcite interface, thus giving rise to the electrical double layer force, which is discussed in the section below.

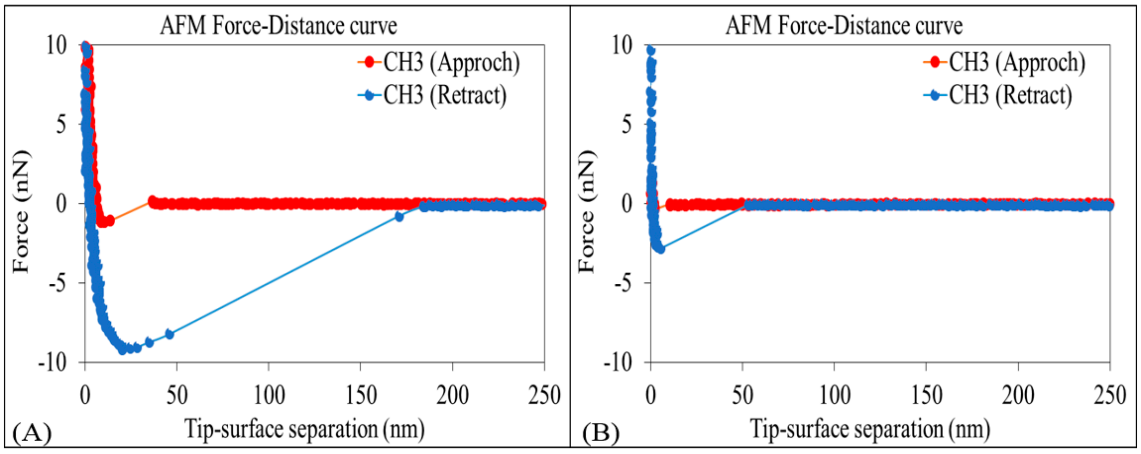

Figure 3. Average force-distance curves of non-polar oil group ($–CH_3$) and calcite in 10,000 ppm NaCl solution at (**A**) pH of 9.5 and (**B**) pH of 11.

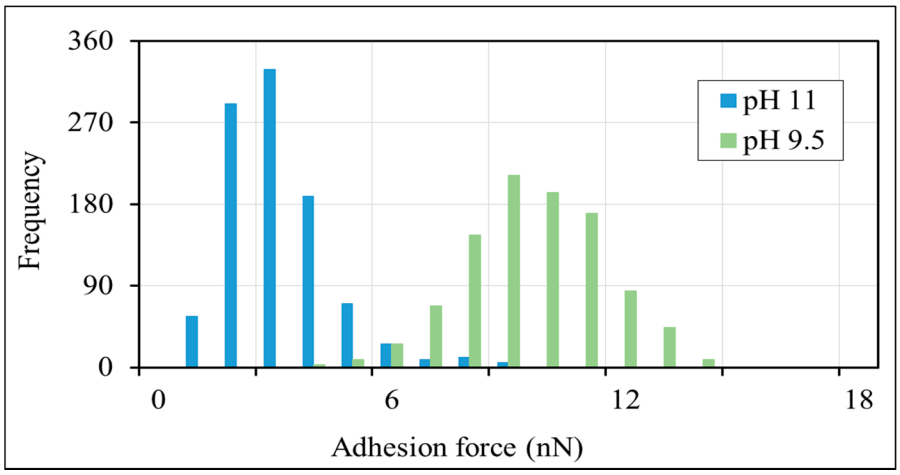

Figure 4. Histograms of adhesion forces between non-polar oil group ($-CH_3$) and calcite in 10,000 ppm NaCl solution at pH of 9.5 and pH of 11.

3.3. *Effect of pH on Zeta Potential of Brine-Calcite and Non-Polar Oil-Brine Interfaces*

The zeta potential of the brine-calcite interface is shifted in the negative direction with increasing pH (Figure 5), which is in line with previous works [68–70]. To be more specific, the zeta potential of the brine-calcite decreases from −8.0 mV to −12.0 mV with increasing pH from 6.5 to 9.5, and decreases further to −18.3 mV when increasing the pH to 11. This is consistent with the work of Thompson et al. [69], who found that increasing the pH from 9 to 11 decreased the zeta potential of the brine-calcite interface from −19 to −31 mV. Similarly, Siffert et al. [68] found that the zeta potential of NaCl brine (1mM)-calcite interface decreased from −2 to −22 mV when increasing pH from 9 to 11. Additionally, Vdovic et al. [70] reported that zeta potential of calcite in 1 mM NaCl brine decreased from −15 to −18 mV when increasing the pH from 9 to 10.5. However, the increase of zeta potential negativity with pH is mainly due to the deprotonation of the calcite surface sites and the increase in the negative calcite surface species $>CaO^-$ and $>CO_3^-$ according to the following geochemical reactions [19,71]:

$$>CaOH^0 + OH^- = >CaO^- + H_2O$$

$$>CO_3H^0 + OH^- = >CO_3^- + H_2O$$

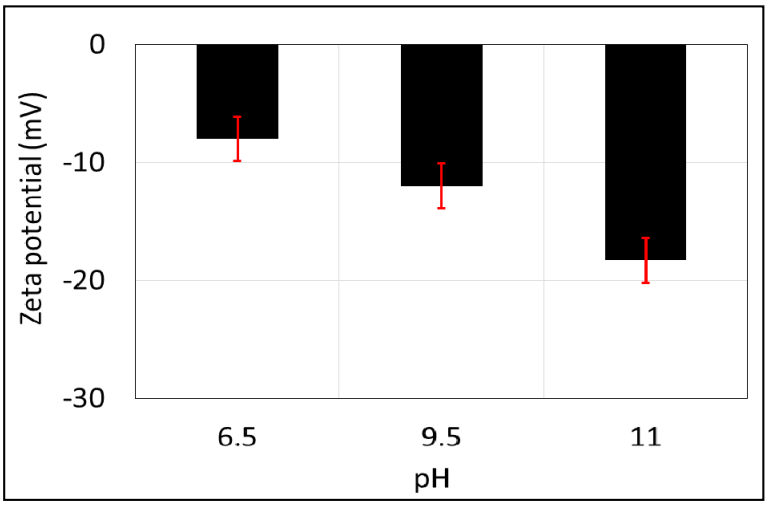

Figure 5. Zeta potential of calcite powder as a function of pH in 10,000 ppm of NaCl solution. Error bars represent the standard deviation.

Similar to the brine-calcite interface, increasing pH yields strongly negative zeta potential of non-polar oil ($–CH_3$)-brine interface. For example, increasing the pH from 6.5 to 9.5 (Figure 6) decreases the zeta potential of the non-polar oil ($–CH_3$)-brine interface from −35 to −45 mV, and it decreases further to −64 mV when increasing the pH to 11. This is consistent with the work of Jozef et al. [72], who observed that increasing the pH from 6 to 11 leads to a decrease in the zeta potential of the non-polar oil (C_6H_{14})-brine from −30 to −35 mV. Also, Marinova et al. [73] observed that raising the pH from 7 to 9 leads to a decrease in the zeta potential of the non-polar oil interface from −70 to −100 mV. Additionally, Beattie et al. [74] reported that zeta potential of the non-polar oil (hexadecane)-brine decreased from −95 to −125 mV when increasing the pH from 7 to 9.5. Taken together, the existing zeta potential of non-polar oil-brine implies that increasing pH leads to the adsorption of excess OH^- on the $–CH_3$ -brine interface, thus further shifting the zeta potential to be more negative [72–74].

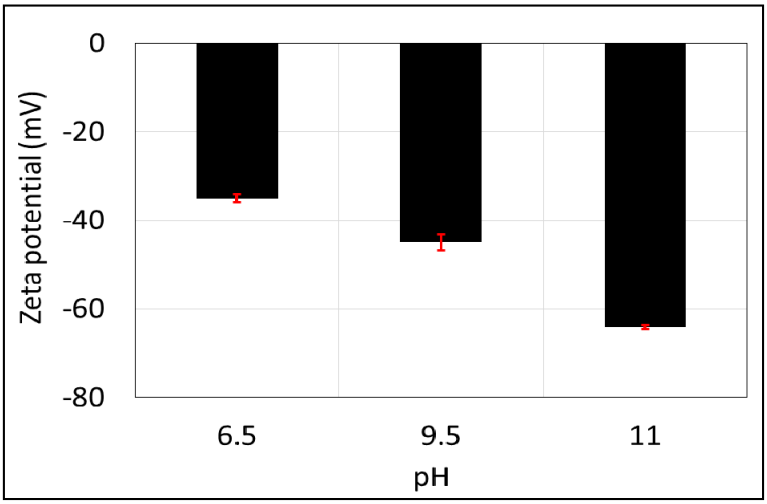

Figure 6. Zeta potential of non-polar oil group ($–CH_3$) as a function of pH in 10,000 ppm of NaCl solution. Error bars represent the standard deviation.

3.4. Effect of pH on Disjoining Pressure of the Sphere to Flat Model

To provide deeper thermodynamic insight into the experiments (e.g., contact angle, AFM adhesion force and zeta potential measurements), total disjoining pressure calculation was performed under constant potential conditions. It is worth noting that positive and negative disjoining pressure represents repulsive and attractive forces, respectively. Figure 7 shows that all pHs (6.5, 9.5 and 11) give negative disjoining pressure (Figure 7) in line with the AFM measurement. Additionally, the total disjoining pressure increases with increasing pH, suggesting greater repulsion in the non-polar oil-brine-calcite systems, which is in agreement with adhesion force results. For example, increasing the pH from 9.5 to 11 increases the repulsion of non-polar oil-brine-calcite systems in line with the AFM measurement.

In general, our results show that increases of pH during low-salinity flooding in carbonate reservoirs lead to detachment of the non-polar oil components (the major oil components) from carbonate surface. This physicochemical process may not be modelled using the existing geochemical reactions because only the polar functional groups are captured in the geochemical models [22,28,75]. However, our results show that the pH increase triggered by low-salinity waterflooding may lead to the detachment of non-polar component. This implies that low-salinity waterflooding may also be applied to carbonate reservoirs with low concentration of polar component such as low acid number and base number.

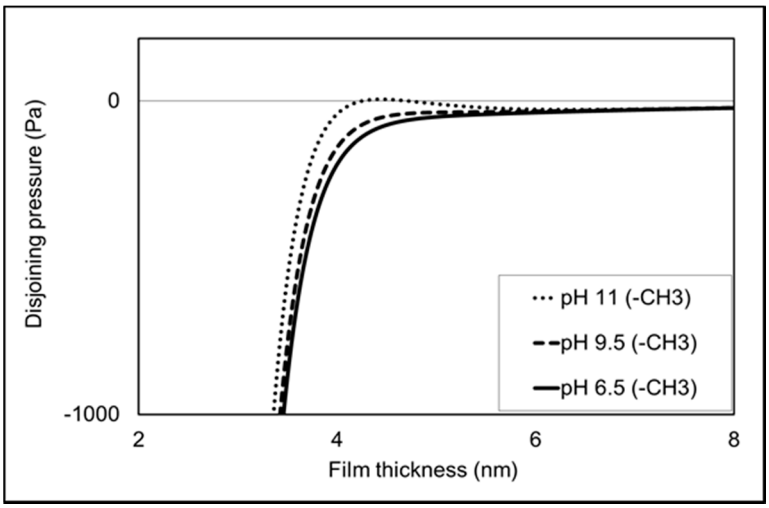

Figure 7. Total disjoining pressure under constant potential conditions versus interfacial separation of calcite and non-polar oil with the presence of NaCl solution at pH 6.5, 9.5 and 11.

4. Summary and Conclusions

Wettability alteration is believed to be a major physicochemical factor in the application of low-salinity water injection in carbonate formations. The effect of polar oil components on wettability alteration has been extensively investigated as a function of pH, but researchers have not evaluated the response of non-polar oil on wettability alteration in much detail, although crude oils are rich in non-polar components. Therefore, we measured the contact angle of non-polar oil on the calcite surface in the presence of an aqueous ionic solution (10,000 ppm NaCl) at pH values of 6.5, 9.5 and 11. In addition, we used atomic force microscopy (AFM) to measure the adhesion of the non-polar oil group ($–CH_3$) and calcite at different pH. Furthermore, to gain a deeper understanding of the isothermal thermodynamic, we performed zeta potential measurements of non-polar oil ($–CH_3$)-brine and brine-calcite interfaces, and calculated the total disjoining pressure using a sphere to flat thermodynamic model under constant potential conditions.

Contact angle measurements showed that the contact angle decreases from 125° to 97° with increasing pH from 6.5 to 9.5, and decreases further, to 78°, when increasing the pH to 11, implying a more water-wet system. AFM adhesion force measurements between the non-polar oil group ($–CH_3$) and calcite showed that the adhesion force decreases with an increase in pH from 9.5 to 11. The zeta potential data measured indicate that an increase in pH would cause a change in the zeta potential of the non-polar oil ($–CH_3$)-brine and calcite-brine interfaces towards more negative values which would then result in an increase in the electrical double layer force. The total disjoining pressure and results of AFM adhesion tests follow similar trends, showing that adhesion force decreases with increasing pH due to electrical double layer expansion thus leads to a water-wet system. Taken together, our results confirm that detachment of non-polar oil from carbonate rock continues to take place during low-salinity water injection, although desorption of non-polar oil from carbonate could not be modeled using existing surface complexation models. Also, this work sheds further light on the significance of pH increase on non-polar oil-calcite adhesion during low-salinity water injection, and provides insights into the quantification of carbonate reservoir wettability.

Author Contributions: Formal analysis, N.S.A.M. and Q.X.; Methodology, N.S.A.M. and A.S.; Project administration, M.M.H.; Software, N.S.A.M.; Supervision, Q.X.; Writing—original draft, N.S.A.M.; Writing—review & editing, A.S. and Q.X. All authors have read and agreed to the published version of the manuscript.

Funding: This research received no external funding

Acknowledgments: The authors would like to acknowledge the substantial support provided by Petroleum Development Oman (PDO). They provided the scholarship and financial support for PhD student Nasser Al Maskari.

Conflicts of Interest: The authors declare no conflict of interest.

References

1. Klemme, H.; Ulmishek, G.F. Effective petroleum source rocks of the world: Stratigraphic distribution and controlling depositional factors. *AAPG Bull.* **1991**, *75*, 1809–1851.
2. Downs, H.H.; Hoover, P.D. Enhanced Oil Recovery by Wettability Alteration. In *Oil-Field Chemistry*; American Chemical Society: Washington, DC, USA, 1989; Volume 396, pp. 577–595.
3. Council, B.E. World Energy Scenarios. In *World Energy Council*; 2013; Available online: https://www.worldenergy.org/assets/downloads/World-Energy-Scenarios_Composing-energy-futures-to-2050_Full-report1.pdf (accessed on 22 December 2019).
4. Al-Shalabi, E.W.; Sepehrnoori, K. A comprehensive review of low salinity/engineered water injections and their applications in sandstone and carbonate rocks. *J. Pet. Sci. Eng.* **2016**, *139*, 137–161. [CrossRef]
5. Al Harrasi, A.; Al-maamari, R.S.; Masalmeh, S.K. Laboratory Investigation of Low Salinity Waterflooding for Carbonate Reservoirs. In Proceedings of the Abu Dhabi International Petroleum Conference and Exhibition, Manama, Bahrain, 25–28 September 2012; Society of Petroleum Engineers: London, UK, 2012.
6. Al-Shalabi, E.W.; Sepehrnoori, K.; Pope, G.; Mohanty, K. A Fundamental Model for Predicting Oil Recovery Due to Low Salinity Water Injection in Carbonate Rocks. In Proceedings of the SPE Energy Resources Conference, Port of Spain, Trinidad and Tobago, 9–11 June 2014; p. 24.
7. Austad, T.; Shariatpanahi, S.F.; Strand, S.; Black, C.J.J.; Webb, K.J. Conditions for a Low-Salinity Enhanced Oil Recovery (EOR) Effect in Carbonate Oil Reservoirs. *Energy Fuels* **2012**, *26*, 569–575. [CrossRef]
8. Mahani, H.; Keya, A.L.; Berg, S.; Bartels, W.-B.; Nasralla, R.; Rossen, W. Driving Mechanism of Low Salinity Flooding in Carbonate Rocks. In Proceedings of the EUROPEC 2015, Madrid, Spain, 1–4 June 2015; p. 27.
9. Nasralla, R.A.; Sergienko, E.; Masalmeh, S.K.; van der Linde, H.A.; Brussee, N.J.; Mahani, H.; Suijkerbuijk, B.M.J.M.; Al-Qarshubi, I.S.M. Potential of Low-Salinity Waterflood To Improve Oil Recovery in Carbonates: Demonstrating the Effect by Qualitative Coreflood. *SPE J.* **2016**, *21*, 1643–1654. [CrossRef]
10. RezaeiDoust, A.; Puntervold, T.; Strand, S.; Austad, T. Smart Water as Wettability Modifier in Carbonate and Sandstone: A Discussion of Similarities/Differences in the Chemical Mechanisms. *Energy Fuels* **2009**, *23*, 4479–4485. [CrossRef]
11. Yousef, A.A.; Al-Saleh, S.; Al-Kaabi, A.; Al-Jawfi, M. Laboratory Investigation of the Impact of Injection-Water Salinity and Ionic Content on Oil Recovery From Carbonate Reservoirs. *SPE Reserv. Eval. Eng.* **2011**, *14*, 578–593. [CrossRef]
12. Yousef, A.A.; Al-Salehsalah, S.H.; Al-Jawfi, M.S. New Recovery Method for Carbonate Reservoirs through Tuning the Injection Water Salinity: Smart WaterFlooding. In Proceedings of the SPE EUROPEC/EAGE annual conference and exhibition, Vienna, Austria, 23–26 May 2011.
13. Alameri, W.; Teklu, T.W.; Graves, R.M.; Kazemi, H.; AlSumaiti, A.M. Wettability Alteration During Low-Salinity Waterflooding in Carbonate Reservoir Cores. In Proceedings of the SPE Asia Pacific Oil & Gas Conference and Exhibition, Adelaide, Australia, 14–16 October 2014; p. 18.
14. Qiao, C.; Li, L.; Johns, R.T.; Xu, J. A Mechanistic Model for Wettability Alteration by Chemically Tuned Water Flooding in Carbonate Reservoirs. In Proceedings of the SPE Annual Technical Conference and Exhibition, Amsterdam, The Netherlands, 27–29 October 2014; p. 29.
15. Shehata, A.M.; Alotaibi, M.B.; Nasr-El-Din, H.A. Waterflooding in Carbonate Reservoirs: Does the Salinity Matter? *SPE Reserv. Eval. Eng.* **2014**, *17*, 304–313. [CrossRef]
16. Zhang, P.M.; Austad, T. Wettability and oil recovery from carbonates: Effects of temperature and potential determining ions. *Colloid Surf. A* **2006**, *279*, 179–187. [CrossRef]
17. Zhang, P.; Tweheyo, M.T.; Austad, T. Wettability alteration and improved oil recovery by spontaneous imbibition of seawater into chalk: Impact of the potential determining ions Ca2+, Mg2+, and SO4 2−. *Colloid Surf. A* **2007**, *301*, 199–208. [CrossRef]
18. Mahani, H.; Keya, A.L.; Berg, S.; Bartels, W.B.; Nasralla, R.; Rossen, W.R. Insights into the Mechanism of Wettability Alteration by Low-Salinity Flooding (LSF) in Carbonates. *Energy Fuels* **2015**, *29*, 1352–1367. [CrossRef]
19. Al Mahrouqi, D.; Vinogradov, J.; Jackson, M.D. Zeta potential of artificial and natural calcite in aqueous solution. *Adv. Colloid Interface Sci.* **2017**, *240*, 60–76. [CrossRef] [PubMed]

20. Alotaibi, M.B.; Nasr-El-Din, H.A.; Fletcher, J.J. Electrokinetics of Limestone and Dolomite Rock Particles. *SPE Reserv. Eval. Eng.* **2011**, *14*, 594–603. [CrossRef]
21. Sari, A.; Chen, Y.Q.; Xie, Q.; Saeedi, A. Low salinity water flooding in high acidic oil reservoirs: Impact of pH on wettability of carbonate reservoirs. *J. Mol. Liq.* **2019**, *281*, 444–450. [CrossRef]
22. Brady, P.V.; Thyne, G. Functional Wettability in Carbonate Reservoirs. *Energy Fuels* **2016**, *30*, 9217–9225. [CrossRef]
23. Mahani, H.; Keya, A.L.; Berg, S.; Nasralla, R. Electrokinetics of carbonate/brine interface in low-salinity waterflooding: Effect of brine salinity, composition, rock type, and pH on ζ-potential and a surface-complexation model. *SPE J.* **2016**. [CrossRef]
24. Liu, F.H.; Yang, H.; Wang, J.Y.; Zhang, M.H.; Chen, T.; Hu, G.X.; Zhang, W.; Wu, J.Z.; Xu, S.J.; Wu, X.; et al. Salinity-dependent adhesion of model molecules of crude oil at quartz surface with different wettability. *Fuel* **2018**, *223*, 401–407. [CrossRef]
25. Abed, J.; Aubry, C.; Zaidani, M.; El Hadri, N.; Devarapalli, R.; Jouiad, M. Determination of Dead-Oil Wetting and Adhesive Forces on Carbonate Rocks Using Colloidal-Probe Atomic Force Microscopy. *Energy Fuels* **2018**, *32*, 9182–9190. [CrossRef]
26. Joonaki, E.; Buckman, J.; Burgass, R.; Tohidi, B. Water versus Asphaltenes; Liquid–Liquid and Solid–Liquid Molecular Interactions Unravel the Mechanisms behind an Improved Oil Recovery Methodology. *Sci. Rep.* **2019**, *9*. [CrossRef]
27. Brady, P.V.; Bryan, C.R.; Thyne, G.; Li, H. Altering wettability to recover more oil from tight formations. *J. Unconv. Oil Gas Resour.* **2016**, *15*, 79–83. [CrossRef]
28. Chen, Y.Q.; Xie, Q.; Sari, A.; Brady, P.V.; Saeedi, A. Oil/water/rock wettability: Influencing factors and implications for low salinity water flooding in carbonate reservoirs. *Fuel* **2018**, *215*, 171–177. [CrossRef]
29. Xie, Q.; Sari, A.; Pu, W.F.; Chen, Y.Q.; Brady, P.V.; Al Maskari, N.; Saeedi, A. pH effect on wettability of oil/brine/carbonate system: Implications for low salinity water flooding. *J. Pet. Sci. Eng.* **2018**, *168*, 419–425. [CrossRef]
30. Qiao, C.H.; Johns, R.; Li, L. Modeling Low-Salinity Waterflooding in Chalk and Limestone Reservoirs. *Energy Fuels* **2016**, *30*, 884–895. [CrossRef]
31. Chandrasekhar, S. Wettability alteration with brine composition in high temperature carbonate reservoirs. In Proceedings of the SPE Annual Technical Conference and Exhibition, New Orleans, LA, USA, 30 September–2 October 2013.
32. Bagci, S.; Kok, M.V.; Turksoy, U. Effect of brine composition on oil recovery by waterflooding. *Pet. Sci. Technol.* **2001**, *19*, 359–372. [CrossRef]
33. Gupta, R.; Smith, G.G.; Hu, L.; Willingham, T.; Lo Cascio, M.; Shyeh, J.J.; Harris, C.R. Enhanced Waterflood for Carbonate Reservoirs—Impact of Injection Water Composition. In Proceedings of the SPE Middle East Oil and Gas Show and Conference, Manama, Bahrain, 25–28 September 2011.
34. Hamouda, A.A.; Gupta, S. Enhancing oil recovery from chalk reservoirs by a low-salinity water flooding mechanism and fluid/rock interactions. *Energies* **2017**, *10*, 576. [CrossRef]
35. Generosi, J.; Ceccato, M.; Andersson, M.P.; Hassenkam, T.; Dobberschütz, S.; Bovet, N.; Stipp, S.L.S. Calcite Wettability in the Presence of Dissolved Mg2+and SO42–. *Energy Fuels* **2016**, *31*, 1005–1014. [CrossRef]
36. Mahani, H.; Menezes, R.; Berg, S.; Fadili, A.; Nasralla, R.; Voskov, D.; Joekar-Niasar, V. Insights into the Impact of Temperature on the Wettability Alteration by Low Salinity in Carbonate Rocks. *Energy Fuels* **2017**, *31*, 7839–7853. [CrossRef]
37. Den Ouden, L.; Nasralla, R.; Guo, H.; Bruining, H.; van Kruijsdijk, C. Calcite dissolution behaviour during low salinity water flooding in carbonate rock. In Proceedings of the IOR 2015—18th European Symposium on Improved Oil Recovery, Dresden, Germany, 14–16 April 2015.
38. Buckley, J.; Liu, Y. Some mechanisms of crude oil/brine/solid interactions. *J. Pet. Sci. Eng.* **1998**, *20*, 155–160. [CrossRef]
39. Xie, Q.; He, S.; Pu, W. The effects of temperature and acid number of crude oil on the wettability of acid volcanic reservoir rock from the Hailar Oilfield. *Pet. Sci.* **2010**, *7*, 93–99. [CrossRef]
40. Gaboriaud, F.; Dufrene, Y.F. Atomic force microscopy of microbial cells: Application to nanomechanical properties, surface forces and molecular recognition forces. *Colloids Surf. B Biointerfaces* **2007**, *54*, 10–19. [CrossRef]

41. Barattin, R.; Voyer, N. Chemical modifications of AFM tips for the study of molecular recognition events. *Chem. Commun.* **2008**, 1513–1532. [CrossRef]
42. Arif, M.; Lebedev, M.; Barifcani, A.; Iglauer, S. CO_2 storage in carbonates: Wettability of calcite. *Int. J. Greenh. Gas Control* **2017**, *62*, 113–121. [CrossRef]
43. Sari, A.; Al Maskari, N.S.; Saeedi, A.; Xie, Q. Impact of surface roughness on wettability of oil-brine-calcite system at sub-pore scale. *J. Mol. Liq.* **2019**. [CrossRef]
44. Al Maskari, N.S.; Sari, A.; Saeedi, A.; Xie, Q. Influence of Surface Roughness on the Contact Angle due to Calcite Dissolution in an Oil–Brine–Calcite System: A Nanoscale Analysis Using Atomic Force Microscopy and Geochemical Modeling. *Energy Fuels* **2019**, *33*, 4219–4224. [CrossRef]
45. Wang, W.; Gupta, A. Investigation of the Effect of Temperature and Pressure on Wettability Using Modified Pendant Drop Method. In Proceedings of the SPE Annual Technical Conference and Exhibition, Dallas, TX, USA, 22–25 October 1995; Society of Petroleum Engineers; p. 10.
46. Alnili, F.; Al-Yaseri, A.; Roshan, H.; Rahman, T.; Verall, M.; Lebedev, M.; Sarmadivaleh, M.; Iglauer, S.; Barifcani, A. Carbon dioxide/brine wettability of porous sandstone versus solid quartz: An experimental and theoretical investigation. *J. Colloid Interface Sci.* **2018**, *524*, 188–194. [CrossRef] [PubMed]
47. Hassenkam, T.; Skovbjerg, L.L.; Stipp, S.L.S. Probing the intrinsically oil-wet surfaces of pores in North Sea chalk at subpore resolution. *Proc. Natl. Acad. Sci. USA* **2009**, *106*, 6071–6076. [CrossRef] [PubMed]
48. Derkani, M.H.; Fletcher, A.J.; Abdallah, W.; Sauerer, B.; Anderson, J.; Zhang, Z.Y.J. Low Salinity Waterflooding in Carbonate Reservoirs: Review of Interfacial Mechanisms. *Colloids Interfaces* **2018**, *2*, 20. [CrossRef]
49. Hassenkam, T.; Andersson, M.P.; Hilner, E.; Matthiesen, J.; Dobberschütz, S.; Dalby, K.N.; Bovet, N.; Stipp, S.L.S.; Salino, P.; Reddick, C.; et al. Could Atomic-Force Microscopy Force Mapping Be a Fast Alternative to Core-Plug Tests for Optimizing Injection-Water Salinity for Enhanced Oil Recovery in Sandstone? *SPE J.* **2016**, *21*. [CrossRef]
50. Shi, L.; Olsson, M.H.M.; Hassenkam, T.; Stipp, S.L.S. A pH-Resolved View of the Low Salinity Effect in Sandstone Reservoirs. *Energy Fuels* **2016**, *30*, 5346–5354. [CrossRef]
51. Wu, J.Z.; Liu, F.H.; Yang, H.; Xu, S.J.; Xie, Q.; Zhang, M.H.; Chen, T.; Hu, G.X.; Wang, J.B. Effect of specific functional groups on oil adhesion from mica substrate: Implications for low salinity effect. *J. Ind. Eng. Chem.* **2017**, *56*, 342–349. [CrossRef]
52. Al Maskari, N.S.; Xie, Q.; Saeedi, A. Role of Basal-Charged Clays in Low Salinity Effect in Sandstone Reservoirs: Adhesion Force on Muscovite using Atomic Force Microscope. *Energy Fuels* **2019**, *33*, 756–764. [CrossRef]
53. Yu, H.A.; Becker, T.; Nic Daeid, N.; Lewis, S.W. Fundamental studies of the adhesion of explosives to textile and non-textile surfaces. *Forensic Sci. Int.* **2017**, *273*, 88–95. [CrossRef] [PubMed]
54. Ron, H.; Matlis, S.; Rubinstein, I. Self-assembled monolayers on oxidized metals. 2. Gold surface oxidative pretreatment, monolayer properties, and depression formation. *Langmuir* **1998**, *14*, 1116–1121. [CrossRef]
55. Fujihira, M.; Tani, Y.; Furugori, M.; Akiba, U.; Okabe, Y. Chemical force microscopy of self-assembled monolayers on sputtered gold films patterned by phase separation. *Ultramicroscopy* **2001**, *86*, 63–73. [CrossRef]
56. Xie, Q.; Liu, F.; Chen, Y.; Yang, H.; Saeedi, A.; Hossain, M.M. Effect of electrical double layer and ion exchange on low salinity EOR in a pH controlled system. *J. Pet. Sci. Eng.* **2019**, *174*, 418–424. [CrossRef]
57. Tian, H.; Liu, F.; Jin, X.; Wang, M. Competitive effects of interfacial interactions on ion-tuned wettability by atomic simulations. *J. Colloid Interface Sci.* **2019**, *540*, 495–500. [CrossRef]
58. Yang, G.; Chen, T.; Zhao, J.; Yu, D.; Liu, F.; Wang, D.; Fan, M.; Chen, W.; Zhang, J.; Yang, H.; et al. Desorption Mechanism of Asphaltenes in the Presence of Electrolyte and the Extended Derjaguin–Landau–Verwey–Overbeek Theory. *Energy Fuels* **2015**, *29*, 4272–4280. [CrossRef]
59. Israelachvili, J.N. Chapter 14—Electrostatic Forces between Surfaces in Liquids. In *Intermolecular and Surface Forces*, 3rd ed.; Israelachvili, J.N., Ed.; Academic Press: Cambridge, MA, USA, 2011; pp. 291–340.
60. Israelachvili, J.N. 15—Solvation, Structural, and Hydration Forces. In *Intermolecular and Surface Forces*, 3rd ed.; Israelachvili, J.N., Ed.; Academic Press: Cambridge, MA, USA, 2011; pp. 341–380.
61. Israelachvili, J.N. Chapter 13—Van der Waals Forces between Particles and Surfaces. In *Intermolecular and Surface Forces*, 3rd ed.; Israelachvili, J.N., Ed.; Academic Press: Cambridge, MA, USA, 2011; pp. 253–289.

62. Juhl, K.M.; Pedersen, C.S.; Bovet, N.; Dalby, K.N.; Hassenkam, T.; Andersson, M.P.; Okhrimenko, D.; Stipp, S.L. Adhesion of alkane as a functional group on muscovite and quartz: Dependence on pH and contact time. *Langmuir* **2014**, *30*, 14476–14485. [CrossRef]
63. Churaev, N.V.; Derjaguin, B.V. Inclusion of Structural Forces in the Theory of Stability of Colloids and Films. *J. Colloid Interface Sci.* **1985**, *103*, 542–553. [CrossRef]
64. Dehghan Monfared, A.; Ghazanfari, M.H.; Kazemeini, M.; Jamialahmadi, M.; Helalizadeh, A. Wettability Alteration Modeling for Oil-Wet Calcite/Silica Nanoparticle System Using Surface Forces Analysis: Contribution of DLVO versus Non-DLVO Interactions. *Ind. Eng. Chem. Res.* **2018**, *57*, 14482–14492. [CrossRef]
65. Kilpatrick, J.I.; Loh, S.-H.; Jarvis, S.P. Directly Probing the Effects of Ions on Hydration Forces at Interfaces. *J. Am. Chem. Soc.* **2013**, *135*, 2628–2634. [CrossRef]
66. Tabor, R.F.; Grieser, F.; Dagastine, R.R.; Chan, D.Y. The hydrophobic force: Measurements and methods. *Phys. Chem. Chem. Phys.* **2014**, *16*, 18065–18075. [CrossRef] [PubMed]
67. Rezaei Gomari, K.A.; Hamouda, A.A. Effect of fatty acids, water composition and pH on the wettability alteration of calcite surface. *J. Pet. Sci. Eng.* **2006**, *50*, 140–150. [CrossRef]
68. Siffert, D.; Fimbel, P. Parameters affecting the sign and magnitude of the eletrokinetic potential of calcite. *Colloids Surf.* **1984**, *11*, 377–389. [CrossRef]
69. Thompson, D.W.; Pownall, P.G. Surface Electrical-Properties of Calcite. *J. Colloid Interface Sci.* **1989**, *131*, 74–82. [CrossRef]
70. Vdović, N. Electrokinetic behaviour of calcite—The relationship with other calcite properties. *Chem. Geol.* **2001**, *177*, 241–248. [CrossRef]
71. Heberling, F.; Trainor, T.P.; Lutzenkirchen, J.; Eng, P.; Denecke, M.A.; Bosbach, D. Structure and reactivity of the calcite-water interface. *J. Colloid Interface Sci.* **2011**, *354*, 843–857. [CrossRef]
72. Stachurski, J.; MichaLek, M. The Effect of the zeta Potential on the Stability of a Non-Polar Oil-in-Water Emulsion. *J. Colloid Interface Sci.* **1996**, *184*, 433–436. [CrossRef]
73. Marinova, K.G.; Alargova, R.G.; Denkov, N.D.; Velev, O.D.; Petsev, D.N.; Ivanov, I.B.; Borwankar, R.P. Charging of Oil–Water Interfaces Due to Spontaneous Adsorption of Hydroxyl Ions. *Langmuir* **1996**, *12*, 2045–2051. [CrossRef]
74. Beattie, J.K.; Djerdjev, A.M. The pristine oil/water interface: Surfactant-free hydroxide-charged emulsions. *Angew. Chem.* **2004**, *43*, 3568–3571. [CrossRef]
75. Chen, Y.; Sari, A.; Xie, Q.; Brady, P.V.; Hossain, M.M.; Saeedi, A. Electrostatic Origins of CO2-Increased Hydrophilicity in Carbonate Reservoirs. *Sci. Rep.* **2018**, *8*. [CrossRef]